

Dynamics Analysis of Cycloidal Speed Reducers With Pinwheel and Nonpinwheel Designs

Chiu-Fan Hsieh

Department of Mechanical and Computer-Aided Engineering,
National Formosa University,
64 Wunhua Road, Huwei,
Yunlin, Taiwan
e-mail: cfhsieh@nfu.edu.tw

Cycloidal speed reducers are composed primarily of an eccentric shaft, output parts, and a set comprising a cycloidal gear and pinwheel with pins or a cycloidal gear and cycloid internal gear. This paper investigates the contact and collision conditions of these components, as well as their stress variations during the transmission process. To do so, a system dynamics analysis model of a cycloidal speed reducer is constructed, together with dynamics analysis models for two design types: A traditional pinwheel design and a nonpinwheel design (i.e., a design in which a cycloid internal gear replaces the pinwheel). Based on the theory of gearing, a mathematical model of the pinwheel with pins, cycloidal gear, and cycloid internal gear is then built from which the component geometry can be derived. These dynamics analysis models, constructed concurrently, are used to investigate the components' movements and stress variations, and determine the differences between the transmission mechanisms. The results indicate that the nonpinwheel design effectively reduces vibration, stress value, and stress fluctuation, thereby enhancing performance. An additional torsion test further suggests that the nonpinwheel design's output rate is superior to that of the traditional pinwheel design.

[DOI: 10.1115/1.4027850]

Keywords: cycloidal speed reducer, gear, kinematics, dynamics, stress

1 Introduction

Cycloid (trochoidal) drives, which are widely used in industry, provide high reduction ratios with low backlash, high accuracy, high efficiency, and high stiffness. In trying to improve their design, researchers have addressed myriad aspects, including the influence of machining tolerances [1,2]; profile generation and analysis, avoidance of undercutting, and design region [3–13]; and calculation of the force distribution on cycloid drive elements, their power losses, and theoretical mechanical efficiency [14–16]. Some recent work has focused particularly on the dynamic behavior of a cycloidal speed reducer [17], proposing a new two-stage design and subjecting it to a stress analysis [18].

Sensinger, after providing a mathematical model of stress, efficiency, and moment of inertia [19], applied Del Castillo's sensitivity framework to derive equations and explain transmission efficiency for wolfrom, cycloid, compound cycloid drives, and harmonic drives. He also developed a method for predicting efficiency based on varied torque ratio, which is useful for identifying the benefits and disadvantages of different types of reducers [20]. Besides, Sensinger and Lipsey [21] found the fixed-pins design lost more energy than free-pins design, and caused the efficiency of fixed-pins design is inferior. They also demonstrated the cycloid drives have greater efficiency over the harmonic drives, and suggested the cycloid drives should be considered for applications in anthropomorphic robots and prostheses. Other recent developments include a model of meshing clearance in a trochoidal gear [22].

The many contributions to the theory of trochoidal drives for geometric (or new) design and analysis include those centered on force and stress, and encompass both efficiency calculations and experiments. All such research indicates that the cycloidal drive is a very important machine component. In this paper, a systematic

dynamics analysis model of the cycloidal speed reducer is developed that can perform not only a kinematic analysis but also a dynamic stress analysis. As a result, the investigation is able to determine both the contact and collision conditions and the stress variations of these components during the transmission process.

To this end, two dynamics analysis models of cycloidal speed reducers are constructed: one for a traditional pinwheel design (pin design) and the other for a design in which the cycloid internal gear replaces the pinwheel (nonpin design). In the latter, the cycloid internal gear is generated by the double-enveloping method first proposed by Hwang and Hsieh [11]. The benefit of this method is that the double contact lines in a certain meshing area can improve the load capacity and transmission precision of the gear reducer, an advantage verified by calculating the relative normal curvature and performing a transmission error test. In addition, the double-enveloping cycloid conjugated tooth pair is superior to the conventional cycloid drive [13], a claim supported here by the results for the dynamics model developed to express transmission characteristics. This model is also able to analyze the influence of dynamics in different designs of the cycloid drive's gear profile.

In Sec. 2, the first outline the mathematical model of the pinwheel (or ring gear housing) with pins, cycloidal gear, and cycloid internal gear and then present the results of the dynamics analyses and torsion test.

2 Design and Analysis of the Geometry

2.1 Mathematical Model of Pin and Nonpin Designs. Figure 1 graphs the generation principle of a cycloidal gear and pinwheel with pins. Here, an extended epitrochoid is traced by a point (p) lying outside the rolling circle that rotates outside of a base circle circumference in a pure rolling motion. If the epitrochoid path is assumed to be the center of the rollers, the cycloidal gear profile can be produced by the inner envelope method. The figure also shows the coordinate systems S_1 , S_2 , and S_f , which are rigidly attached to the pinwheel, cycloidal gear, and frame, respectively.

Contributed by the Power Transmission and Gearing Committee of ASME for publication in the JOURNAL OF MECHANICAL DESIGN. Manuscript received January 25, 2014; final manuscript received June 5, 2014; published online June 26, 2014. Associate Editor: Zhang-Hua Fong.

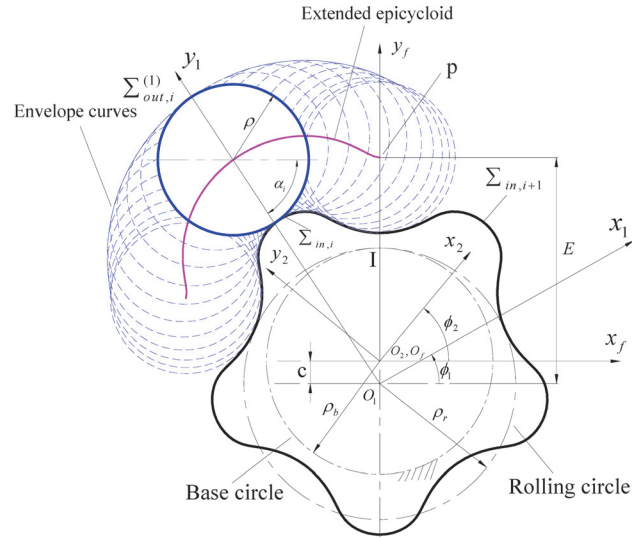


Fig. 1 Generation principle of cycloidal gear and pin wheel with pins

Because the pinwheel has one more tooth than the cycloidal gear, the ratio of the cycloid gear's rotation angle to that of the pinwheel is inversely proportional to the ratio of the tooth number. Hence, the relation between rotation angle ϕ_2 and ϕ_1 can be represented as

$$\phi_2(\phi_1) = \frac{N}{N-1} \phi_1 \quad (1)$$

where N is the tooth number of the pinwheel. If the pin teeth of the pinwheel are represented in S_1 as

$$\mathbf{r}_1(\alpha_i) = \begin{bmatrix} x_1(\alpha_i) \\ y_1(\alpha_i) \\ 1 \end{bmatrix} = \begin{bmatrix} E \sin \zeta_i + \rho \sin(\alpha_i + \zeta_i) \\ E \cos \zeta_i - \rho \cos(\alpha_i + \zeta_i) \\ 1 \end{bmatrix}, \quad i = 1 \sim N \quad (2)$$

where $\zeta_i = 2\pi(i-1)/N$, then the equation of the cycloid gear can be determined by the following coordinate transformation:

$$\mathbf{r}_2(\alpha_i, \phi_1) = \mathbf{M}_{21}(\phi_1) \mathbf{r}_1(\alpha_i) \quad (3)$$

where

$$\mathbf{M}_{21}(\phi_1) = \begin{bmatrix} \cos(\phi_1 - \phi_2) & -\sin(\phi_1 - \phi_2) & -c \sin \phi_2 \\ \sin(\phi_1 - \phi_2) & \cos(\phi_1 - \phi_2) & -c \cos \phi_2 \\ 0 & 0 & 1 \end{bmatrix}$$

Equation (3) then yields the mathematical equation of the cycloid gear

$$\mathbf{r}_2(\alpha_i, \phi_1) = \begin{bmatrix} x_2(\alpha_i, \phi_1) \\ y_2(\alpha_i, \phi_1) \\ 1 \end{bmatrix} = \begin{bmatrix} E \sin(\zeta_i - \phi_1 + \phi_2) + \rho \sin(\alpha_i + \phi_1 - \phi_2 - \zeta_i) - c \sin \phi_2 \\ E \cos(\zeta_i - \phi_1 + \phi_2) - \rho \cos(\alpha_i + \phi_1 - \phi_2 - \zeta_i) - c \cos \phi_2 \\ 1 \end{bmatrix}, \quad i = 1 \sim N \quad (4)$$

The equation of meshing is represented as in Ref. [23]

$$f_1(\alpha_i, \phi_1) = \left(\frac{\partial \mathbf{r}_1}{\partial \alpha_i} \times \mathbf{k} \right) \cdot \mathbf{V}_1^{(12)} = \mathbf{N}_1 \cdot \mathbf{V}_1^{(12)} = 0 \quad (5)$$

where the sliding velocity, $\mathbf{V}_1^{(12)}$, is

$$\mathbf{V}_1^{(12)} = \mathbf{V}_{x1}^{(12)} + \mathbf{V}_{y1}^{(12)} = \left[(\omega_1^{(1)} - \omega_1^{(2)}) \times \mathbf{r}_1 \right] - (\mathbf{R}_1 \times \omega_1^{(2)}) \quad (6)$$

Here

$$\omega_1^{(1)} = \mathbf{k}$$

$$\omega_1^{(2)} = \frac{N}{N-1} \mathbf{k}$$

$$\mathbf{R}_1 = [c \sin \phi_1 \quad c \cos \phi_1 \quad 1]^T$$

with \mathbf{k} being the unit vector in the z direction. Substituting Eqs. (2) and (6) into Eq. (5) yields the following:

$$f_1(\alpha_i, \phi_1) = E \sin \alpha_i - cN \sin(\alpha_i + \phi_1 - \zeta_i) = 0 \quad (7)$$

Equations (4) and (7) considered simultaneously determine the generated tooth profile of the cycloid gear.

The generation principle of the cycloid internal gear is illustrated in Fig. 2, in which a lobe profile of the cycloid internal gear is formed by the profiles $\sum_{out,i}^{(1)}$, an arc curve, and $\sum_{out,i}^{(2)}$, obtainable using the envelope of the cycloid gear profile (also known as double-enveloping) [11]. The figure also shows the coordinate systems S_a and S_b , which are rigidly attached to the cycloid gear and cycloid internal gear, respectively.

The equation of the cycloid gear (Eq. (4)) in S_a is written as $\mathbf{r}_a(\alpha, \phi_1)$ and, as for Eq. (3), the equation of the cycloid internal gear profile can be determined through coordinate transformation

$$\mathbf{r}_b(\alpha_i, \phi_1, \theta_1) = \mathbf{M}_{ba}(\psi_1) \mathbf{r}_a(\alpha_i, \phi_1)$$

$$\begin{aligned} &= \begin{bmatrix} E \sin(\zeta_i - \phi_1 + \phi_2 - \psi_1 + \psi_2) + \rho \sin(\alpha_i + \phi_1 - \phi_2 + \psi_1 - \psi_2 - \zeta_i) - c[\sin \psi_2 - \sin(\psi_1 - \psi_2 - \phi_2)] \\ E \cos(\zeta_i - \phi_1 + \phi_2 - \psi_1 + \psi_2) - \rho \cos(\alpha_i + \phi_1 - \phi_2 + \psi_1 - \psi_2 - \zeta_i) - c[\cos \psi_2 + \cos(\psi_1 - \psi_2 - \phi_2)] \\ 1 \end{bmatrix} \end{aligned} \quad (8)$$

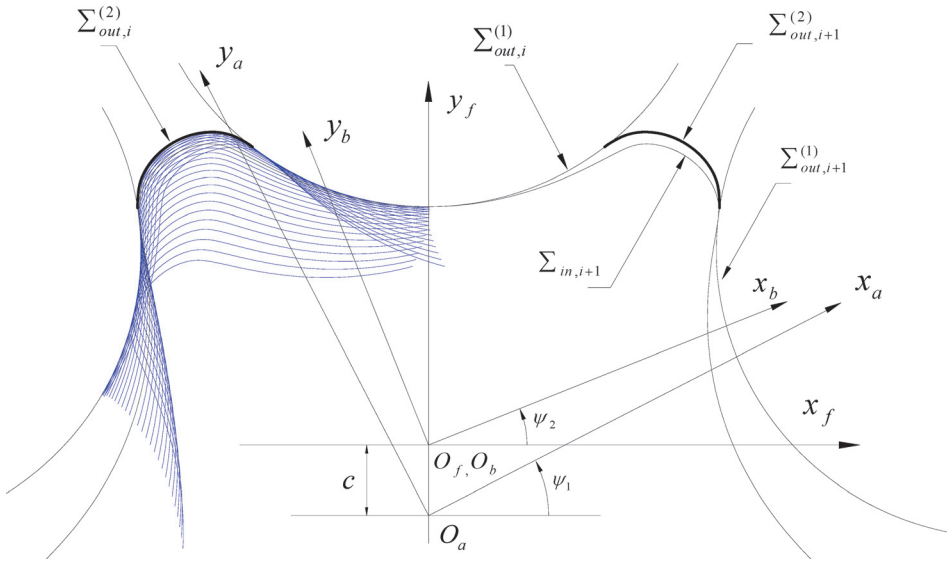


Fig. 2 Generation principle of cycloid internal gear

where

$$\psi_2 = \frac{N-1}{N} \psi_1$$

$$\mathbf{M}_{ba}(\theta_1) = \begin{bmatrix} \cos(\psi_1 - \psi_2) & -\sin(\psi_1 - \psi_2) & -c \sin \psi_2 \\ \sin(\psi_1 - \psi_2) & \cos(\psi_1 - \psi_2) & -c \cos \psi_2 \\ 0 & 0 & 1 \end{bmatrix}$$

The cycloid internal gear tooth profile can then be obtained by simultaneously considering the equation of meshing [23]

$$f_2(x_i, \phi_1, \psi_1) = \left(\frac{\partial \mathbf{r}_a}{\partial \phi_1} \times \mathbf{k} \right) \cdot \mathbf{V}_a^{(ab)} = \mathbf{N}_a \cdot \mathbf{V}_a^{(ab)} = 0 \quad (9)$$

with the sliding velocity, $\mathbf{V}_a^{(ab)}$, represented as

$$\mathbf{V}_a^{(ab)} = \mathbf{V}_{xa}^{(ab)} + \mathbf{V}_{ya}^{(ab)} = \left[(\omega_a^{(a)} - \omega_a^{(b)}) \times \mathbf{r}_a \right] - (\mathbf{R}_a \times \omega_a^{(b)}) \quad (10)$$

where

$$\omega_a^{(a)} = \mathbf{k}$$

$$\omega_a^{(b)} = \frac{N-1}{N} \mathbf{k}$$

$$\mathbf{R}_a = [c \sin \psi_1 \quad c \cos \psi_1 \quad 1]^T$$

Substituting Eqs. (4) and (10) into Eq. (9) yields

$$f_2(x_i, \phi_1, \psi_1) = \sin(\phi_2 - \psi_1) - \frac{E}{cN} \left[\sin(\zeta_i - \phi_1) + \sin(\zeta_i - \phi_1 + \phi_2 - \psi_1) \right] - \frac{\rho}{cN} \left[\sin(\alpha_i - \zeta_i + \phi_1) + \sin(\alpha_i - \zeta_i + \phi_1 - \phi_2 + \psi_1) \right] = 0 \quad (11)$$

2.2 Model Design. The two sets of cycloidal speed reducers designed for this study have one tooth difference. Figure 3 shows the transmission mechanism of the traditional cycloidal pinwheel using a reduction ratio of 35:1. In this pin design, the cycloidal

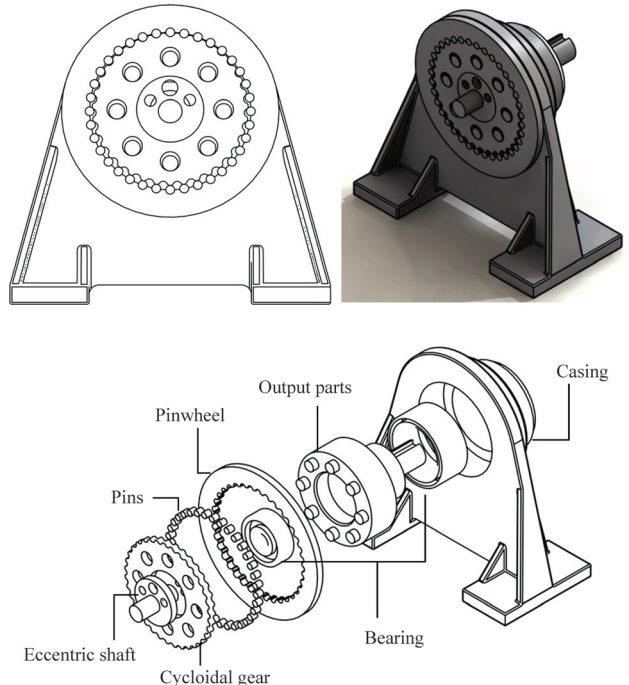


Fig. 3 Reducer with pinwheel design: (a) front view, (b) 3D view, and (c) exploded view

gear has 35 teeth, and the pinwheel has 36 pins. Figure 4 shows the nonpin design significantly differs from the pin design because it uses a cycloid internal gear containing 36 teeth instead of a pinwheel. The design parameter values are thus $N = 36, c = 1, E = 40.75$, and $\rho = 2.25$. In both models, the cam on the eccentric shaft includes a counterweight design and the tolerance is set at 0.001 mm to approximate practical motion.

The cycloidal speed reducer has four primary mechanisms that govern its movement: an eccentric shaft, output parts, and a set comprising either a cycloidal gear and pinwheel with pins or a cycloid internal gear and cycloid internal gear (nonpin design). As the input shaft turns, the eccentric bearing drives the cycloidal gear

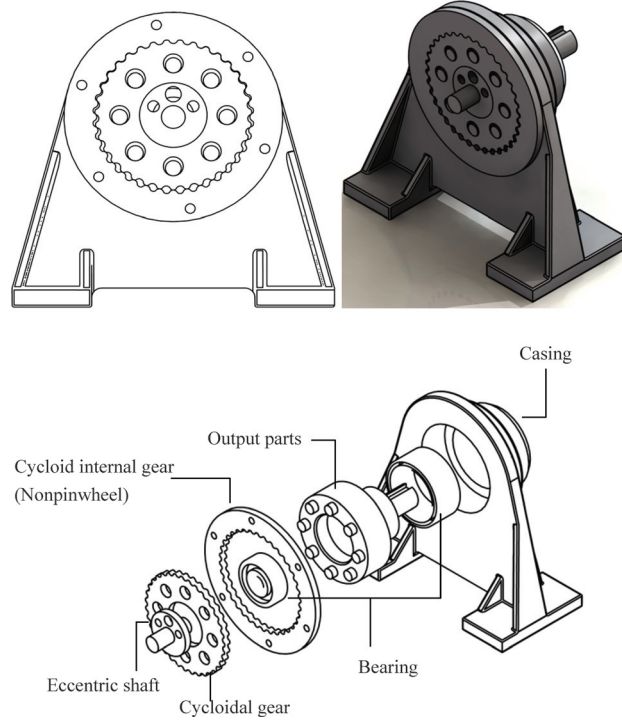


Fig. 4 Reducer with nonpinwheel design: (a) front view, (b) 3D view, and (c) exploded view

into a planetary motion inside the confined pinwheel (or ring gear housing) with pins (Fig. 3). During this process, the cycloidal gear rotates in one direction relative to its own center but advances in the opposite direction relative to the center of the speed reducer. At the same time, several output shaft pins placed inside the small circles of the cycloidal gear convert the wobbling motion of the cycloidal gear into the smooth concentric movement of an output shaft. This feature ultimately reduces the speed and increases the torque.

2.3 Mathematical Model for the Dynamics Analysis. The angular velocity of the cycloidal gear ω_c can be determined by

$$\omega_c = -\frac{\omega_i}{SR} \quad (12)$$

where ω_i is the angular velocity of the input shaft and SR is the reduction ratio. The translational velocity of the cycloidal gear can then be expressed as

$$v_c = c\omega_c \quad (13)$$

and its translational acceleration as

$$a_c = c\omega_c^2 \quad (14)$$

The action force of the cycloidal gear is represented by

$$F_c = m_c a_c \quad (15)$$

where m_c is the weight of the cycloidal gear.

During the motion of the reducer, a circle hole on the cycloidal gear and its center position $q(q_x, q_y)$ form a trajectory curve, meaning that its equation can be represented as

$$\mathbf{R}_q = \begin{bmatrix} q_x \cos \zeta + q_y \sin \zeta - c \sin((N-1)\zeta) \\ q_y \cos \zeta - q_x \sin \zeta + c[\cos((N-1)\zeta) - 1] \\ 1 \end{bmatrix} \quad (16)$$

where, ζ is the gear's revolution angle. To obtain the translational velocity of hole q 's center, Eq. (16) can be differentiated by time t

$$\mathbf{v}_q = \frac{\partial \mathbf{R}_q}{\partial t} = \begin{bmatrix} v_{qx} \\ v_{qy} \\ 0 \end{bmatrix} = \begin{bmatrix} [q_y \cos \zeta - q_x \sin \zeta + c(N-1) \cos((N-1)\zeta)]\omega_c \\ [-q_x \cos \zeta - q_y \sin \zeta + c(N-1) \sin((N-1)\zeta)]\omega_c \\ 0 \end{bmatrix} \quad (17)$$

$$\omega_c = \frac{d\zeta}{dt}$$

and the translational velocity determined as follows:

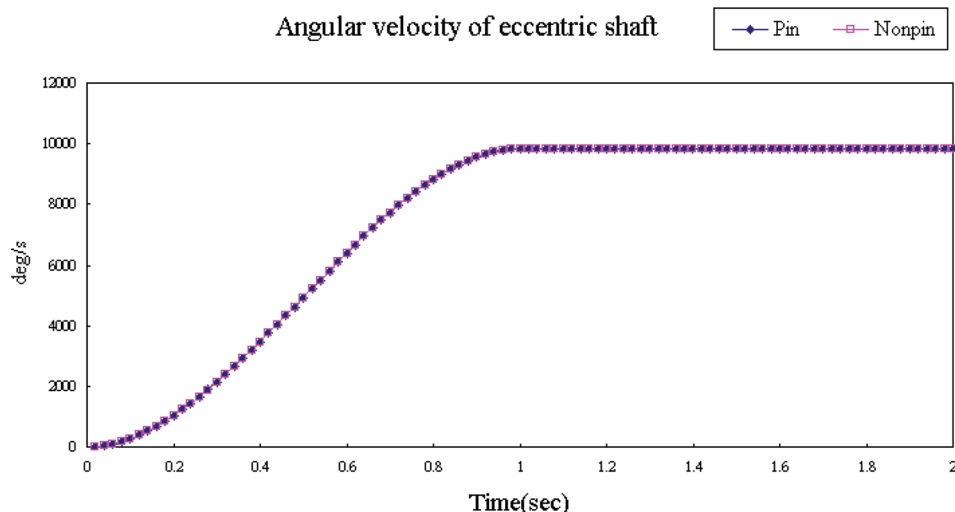


Fig. 5 Angular velocity of eccentric shaft

Table 1 Mechanical properties of material (unit: N/mm²)

Mechanical properties	Elastic modulus	Shear modulus	Tensile strength	Yield strength
Material: Alloy steel	210,000	79,000	723.1025	620.422

$$\begin{aligned} v_q &= \sqrt{v_{qx}^2 + v_{qy}^2} \\ &= \omega_c \sqrt{(c(N-1))^2 + (q_x^2 + q_y^2) - 2c(N-1)(q_y \cos(N\zeta) - q_x \sin(N\zeta))} \end{aligned} \quad (18)$$

Likewise, to obtain the translational acceleration of hole q 's center, Eq. (17) can be differentiated by time t

$$\begin{aligned} \mathbf{a}_q &= \frac{\partial \mathbf{v}_q}{\partial t} = \begin{bmatrix} a_{qx} \\ a_{qy} \\ 0 \end{bmatrix} \\ &= \begin{bmatrix} [-q_x \cos \zeta - q_y \sin \zeta + c(N-1)^2 \sin((N-1)\zeta)] \omega_c^2 \\ [-q_y \cos \zeta + q_x \sin \zeta - c(N-1)^2 \cos((N-1)\zeta)] \omega_c^2 \\ 0 \end{bmatrix}, \end{aligned} \quad (19)$$

$$\omega_c^2 = \frac{d^2 \zeta}{dt^2}$$

and the translational acceleration determined as follows:

$$\begin{aligned} a_q &= \sqrt{a_{qx}^2 + a_{qy}^2} \\ &= \omega_c^2 \sqrt{c^2(N-1)^4 + q_x^2 + q_y^2 - 2c(N-1)^2(q_y \cos(N\zeta) - q_x \sin(N\zeta))} \end{aligned} \quad (20)$$

Because the reducer is a systematic multibody mechanism, the dynamics equation can be expressed as [24]

$$\kappa \mathbf{s}^T (\mathbf{F}(t) - \mathbf{M} \ddot{\mathbf{s}}) = 0 \quad (21)$$

$$\mathbf{M} \ddot{\mathbf{s}} + \boldsymbol{\Omega}_s^T \boldsymbol{\lambda} = \mathbf{F}(t) \quad (22)$$

where κ is the systematic degree of freedom, $\boldsymbol{\Omega}_s^T$ is a Jacobin matrix of the kinematics constraint equation, $\boldsymbol{\lambda}$ is a Lagrange multipliers matrix, and \mathbf{s} , \mathbf{M} , and $\mathbf{F}(t)$ are, respectively, a multibody generalized coordinates matrix, a generalized mass matrix, and a generalized force matrix expressible as

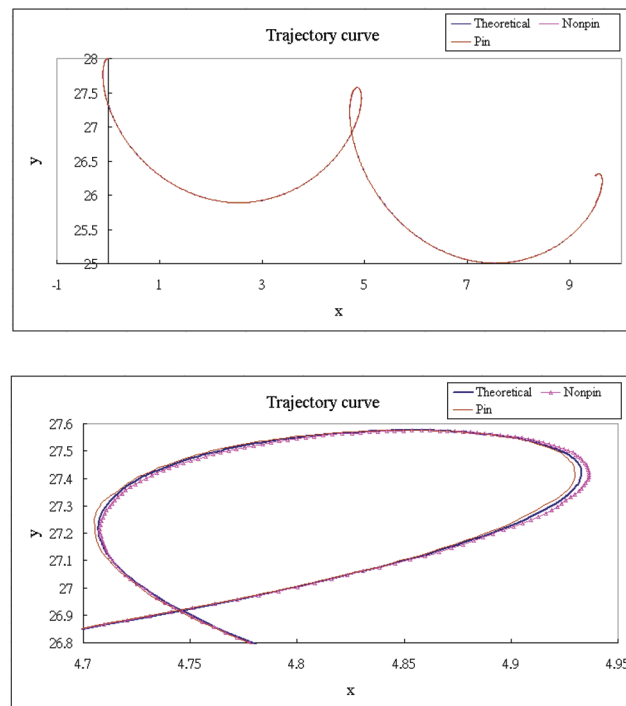
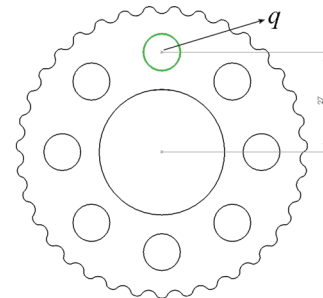


Fig. 7 Trajectory curve of point q : (a) point q indication, (b) three trajectory curves, and (c) local amplification

$$\mathbf{s} = \begin{bmatrix} \mathbf{s}_1 \\ \vdots \\ \mathbf{s}_n \end{bmatrix}, \quad \mathbf{F}(t) = \begin{bmatrix} \mathbf{F}_1(t) \\ \vdots \\ \mathbf{F}_n(t) \end{bmatrix}, \quad \mathbf{M} = \begin{bmatrix} m_1 & \cdots & 0 \\ \vdots & \ddots & \vdots \\ 0 & \cdots & m_n \end{bmatrix} \quad (23)$$

If the multibody system has u number of constraints, then the constraint equation $\boldsymbol{\Omega}$ can be expressed as

$$\boldsymbol{\Omega}(\mathbf{s}, t) = 0 \quad (24)$$

where $\boldsymbol{\Omega}$ is a constraint equation matrix

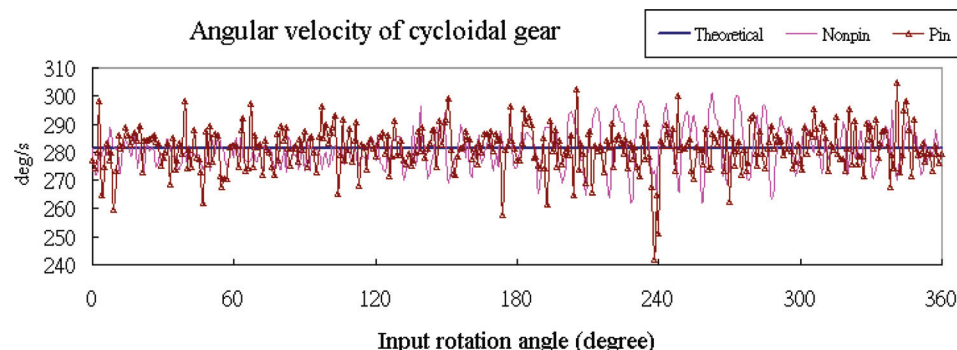


Fig. 6 Angular velocity of cycloidal gear

$$\boldsymbol{\Omega} = [\boldsymbol{\Omega}_1 \dots \boldsymbol{\Omega}_u]^T \quad (25)$$

The latter yields the following constraint equations of velocity and acceleration:

$$\boldsymbol{\Omega}_s \dot{s} + \frac{\partial \boldsymbol{\Omega}}{\partial t} = 0 \quad (26)$$

$$\boldsymbol{\Omega}_s \ddot{s} + \frac{\partial(\boldsymbol{\Omega}_s \dot{s})}{\partial s} \dot{s} + 2 \frac{\partial \boldsymbol{\Omega}_s}{\partial t} + \frac{\partial \boldsymbol{\Omega}_t}{\partial t} = 0 \quad (27)$$

where

$$\boldsymbol{\Omega}_s = \frac{\partial \boldsymbol{\Omega}}{\partial s}, \boldsymbol{\Omega}_t = \frac{\partial \boldsymbol{\Omega}}{\partial t} \quad (28)$$

The above dynamics and constraint equations allow solution of the dynamics analysis.

3 Results and Discussions

3.1 Conditions of the Dynamic Simulation. In this paper, the dynamic analysis was carried out by theoretical calculation (using the math model in Sec. 2.3) and simulation using SolidWorks COSMOS. Assuming an input power of 0.18 kW, the rotational speed is 1640 rpm (i.e., 9840 deg/s) and the input torque 1.048 N m. The given movement curve for the eccentric shaft is as shown in Fig. 5: The acceleration phase occurs between 0 and 1 s, and the velocity is constant after 1 s. Assuming that the output shaft has no added load (i.e., is no-load running), the contact mode of the parts is a 3D collision and the gravitational acceleration is 9.8 m/s^2 (in consideration of gravitational forces). The parts are made of alloy steel, and the relevant mechanical properties are as listed in Table 1.

To prove the feasibility of the dynamic model, a small time-step is carried out by operating at a constant velocity (1640 rpm). The results indicate that the input shaft rotates one round, the data are solved at every angle, the interval angle is 1 deg, and the interval time is 0.000101626 s. Sections 3.2 and 3.3 discuss these results for each component part.

3.2 Kinematic Analysis. Because the cycloidal gear is a core part of the reducer, understanding its motion condition allows prediction of its motion performance. In fact, in Fig. 6 graph of the cycloidal gear's angular velocity indicates a greater fluctuation for the pin design because of part collision. Such collision is possible because in the pin design model, the pins on the pinwheel can spin freely and collide with the cycloidal gear and pinwheel. The trajectory of point q on the cycloidal gear, however, suggests that in both the theoretical and simulation results, transmission errors occur in both designs because of different collision modes during reducer operation (Fig. 7(a)). That is, in the pin design, the cycloidal gear collides with the pins, whereas in the nonpin design, the cycloidal gear collides with the cycloid internal gear. Given this difference in contact mode, the velocity of point q fluctuates but is more pronounced in the pin than the nonpin design (Fig. 8). In general, therefore, the velocity analysis indicates that the pin design leads to larger motion variation and causes more vibration.

In this paper, the model can successfully approximate a practical rotating situation. Figure 9(a) presents four input rotation angles: 0 deg, 120 deg, 240 deg, and 360 deg. Because of the motion relationship, the input shaft drives the cycloidal gear into revolution and a rotation movement, thereby forcing the pins to spin (see Fig. 9(a)). The pins also sway slightly because of collision. Taking the pin 1 in Fig. 9(a) as an example, Fig. 9(b) shows the variation in its center position. These results show why this pin design has a more fluctuation motion and may make more vibration and noise. In the nonpin design, in contrast, because of

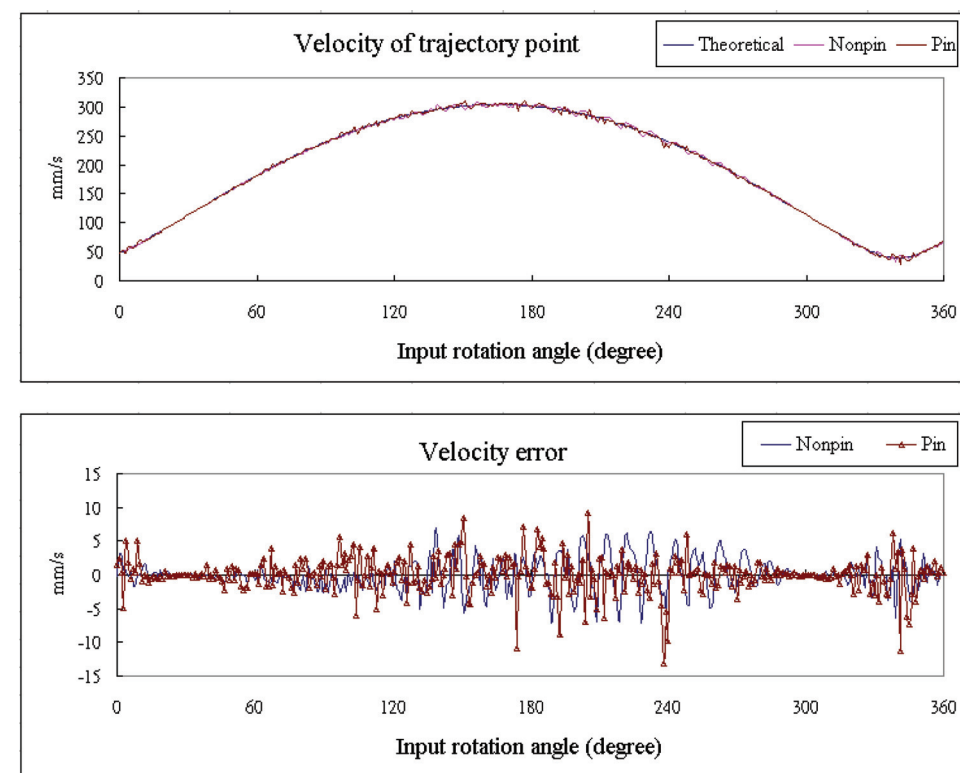


Fig. 8 Velocity analysis of point q : (a) three velocity curves and (b) error = simulation – theoretical

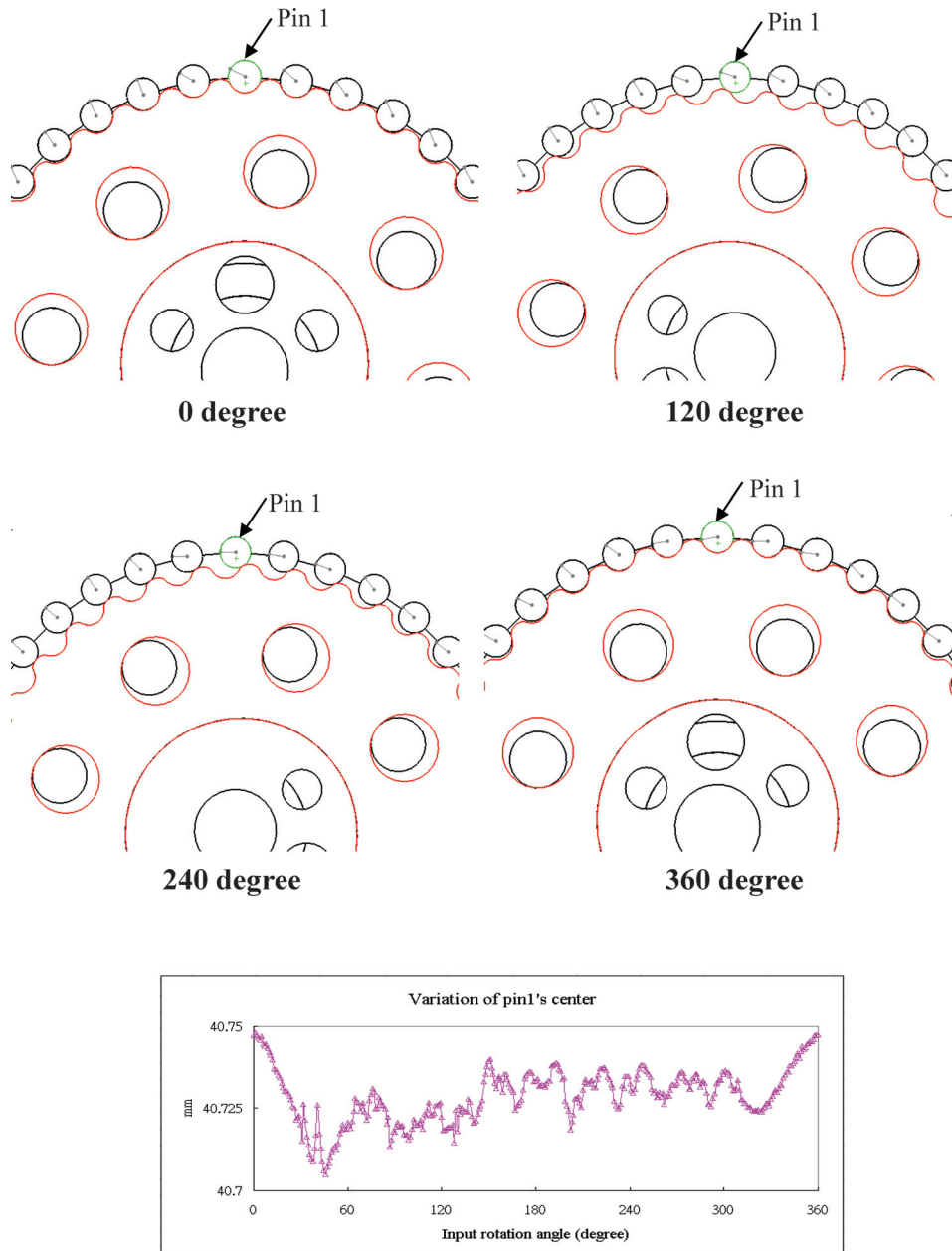


Fig. 9 Variation of the pin 1's center: (a) spin of pins and (b) $\sqrt{C_x^2 + C_y^2}$

fluctuations in velocity, vibration is comparatively smaller and the rotation substantially more stable.

3.3 Stress Analysis. The stress variation of the cycloidal speed reducer during movement can be calculated using the finite element method. In this study, the primary parts analyzed are the eccentric shaft, output parts, cycloidal gear, pinwheel, and cycloid internal gear. Take the pin design as an example; first, a triangular grid calculation must be performed by conducting a grid calculation on each part at a certain time (see Fig. 10). Subsequently, the stress conditions of each part can be identified according to the color difference diagram (Fig. 11). Based on these calculations, the primary parts of the pin and nonpin designs can be compared and the differences identified.

In the pin design, because the tiny clearances exist between the pins and the pin wheel, the pins on the pinwheel can freely spin and collide with other components. Hence, when the eccentric shaft operates at high speed and drives the cycloidal gear, collision occurs both between the cycloidal gear and the pins and

between the pins and the pinwheel. As a result, the pins sway slightly and significantly influence the dynamics or power transfer of the mechanism's entire system. The analysis of stress fluctuation below explains this phenomenon in more detail.

Figure 12 graphs the stress analysis of the eccentric shaft, showing clearly that the stress value and fluctuation in the pin design is larger than those in the nonpin design. Especially, larger stress pulsation would arise at two positions which are nearby 75 deg and 255 deg. The maximum stress would take place when the input shaft rotates at 74 deg angle. At this moment, the stress diagram at each part can also be shown in Fig. 11. The stress analyses of the cycloidal gear and pinwheel also indicate fewer fluctuations and smaller average stress values in the nonpin design than in the pin design (Figs. 13 and 14). Because in this model, the output end is set to be no load—meaning that the output parts are driven by the wobbling motion of the cycloidal gear—the stress values in these parts are lower and the fluctuation regular (Fig. 15).

As shown in Fig. 16, according to the stress analysis of the pin 1 (see Fig. 9(a)), when the input shaft rotates 0 deg, the cycloidal



Fig. 10 Grid calculation: (a) eccentric shaft, (b) output parts, and (c) gears of pin design

gear runs over the pin 1, a state of collision and pressure that increases the stress. At less than a 10 deg angle, the pressure is gradually relieved as the rotating angle increases, causing the stress to gradually decrease. The pin 1 then enters a state of sliding friction with the cycloidal gear until about 350 deg, at which

time another pressure state ensues, the stress increases gradually until 360 deg, and the stress cycle completes. The stress value of the pin 1, therefore, manifests regular and periodic variation when the input shaft rotates more cycles.

The analysis of stress magnitude (Figs. 12–14) reveals that, because of the cycloidal gear's position (on top of the eccentric shaft), it collides and makes contact with the pins (or cycloid internal gear) regardless of design (pin or nonpin). Based on this rotation, the relation among the different parts in terms of stress magnitude can be described as follows: eccentric shaft > pinwheel (or cycloid internal gear) > cycloidal gear.

According to Fig. 12, the stress value of the eccentric shaft in the pin design fluctuates below approximately 160 MPa, whereas that in the nonpin design fluctuates below approximately 60 MPa. For the cycloidal gear (Fig. 13), the stress value in the pin design fluctuates below approximately 20 MPa, while that in the nonpin design fluctuates below approximately 10 MPa. Figure 14 shows the stress values of the pinwheel and cycloid internal gear in the pin and nonpin design, respectively. The stress value of the pinwheel in the pin design fluctuates below approximately 65 MPa, whereas that of the cycloid internal gear in the nonpin design fluctuates below approximately 50 MPa (Fig. 14).

Hence, both the movement analysis and the stress analysis indicate that the vibrations, stress fluctuations, and stress values in the nonpin design are smaller than those in the pin design, meaning that the former performs better than the latter. Moreover, in an additional simulation of output torque, the value in the nonpin design, at 35.8 N m, is higher than that in the pin design (34.7 N m). These results can be used as indicators for assessing speed reducer performance. In fact, as described below, this torsion test was applied in the manufacture of entire speed reducer mechanisms to verify the accuracy of the proposed assessment method.

3.4 Experimental Results. The manufacture of the main parts used in this study is illustrated in Fig. 17; the equipment

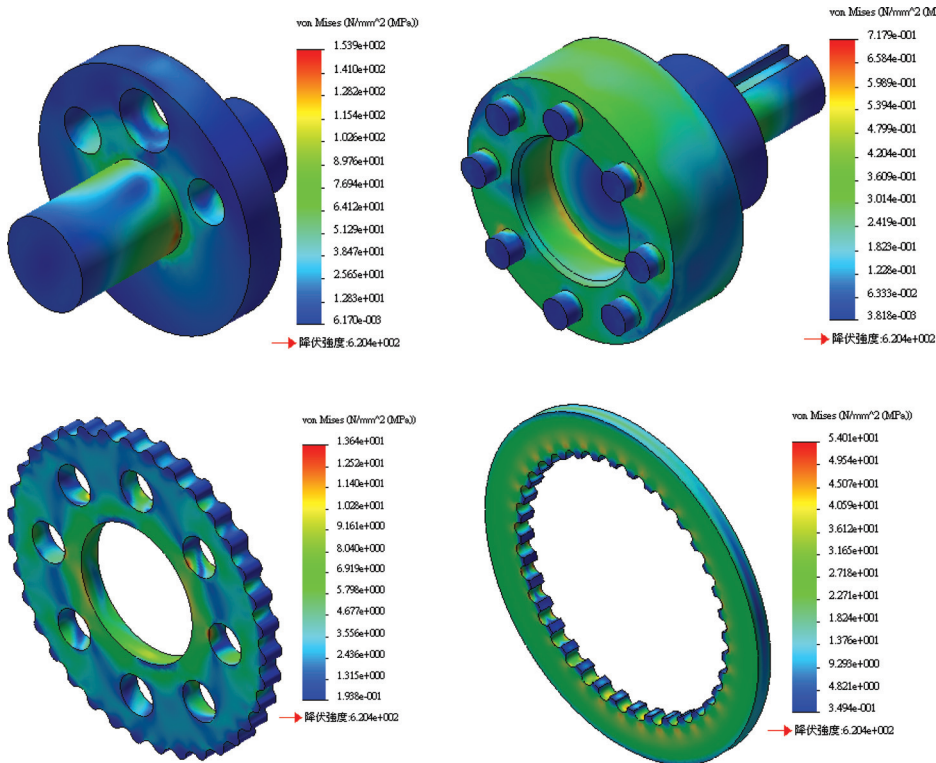


Fig. 11 Stress calculation (input rotation angle at 74 deg): (a) eccentric shaft, (b) output parts, and (c) gears of pin design

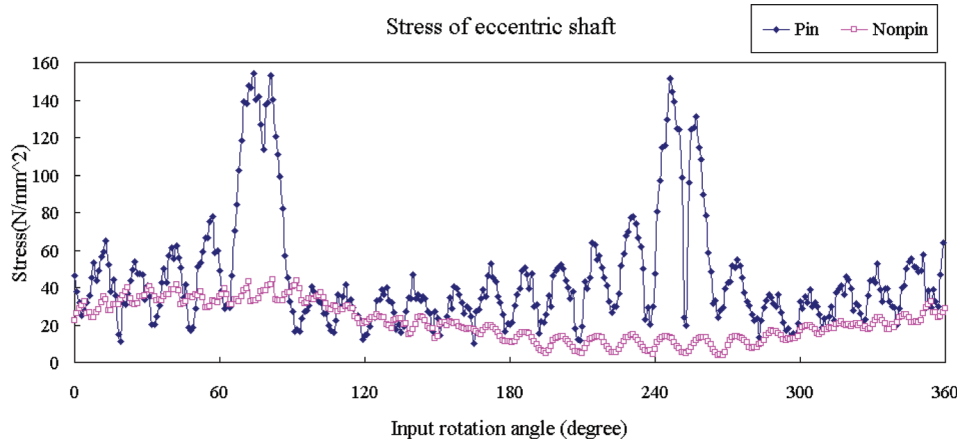


Fig. 12 Stress of eccentric shaft

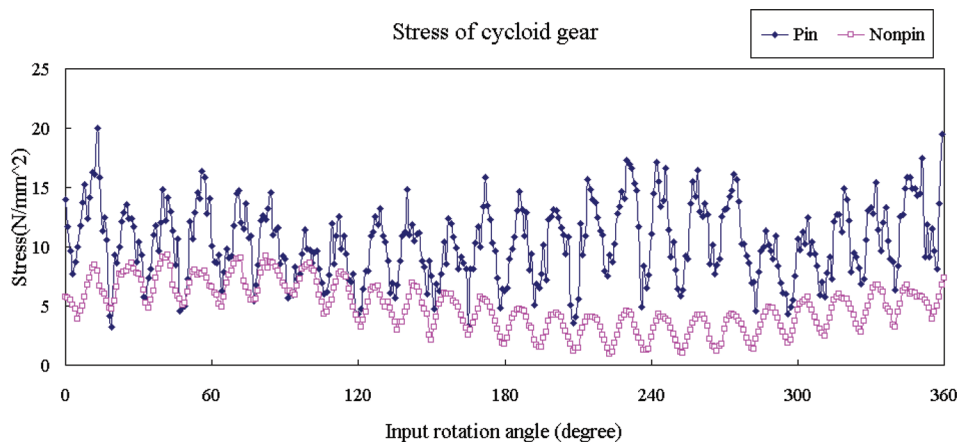


Fig. 13 Stress of cycloidal gear

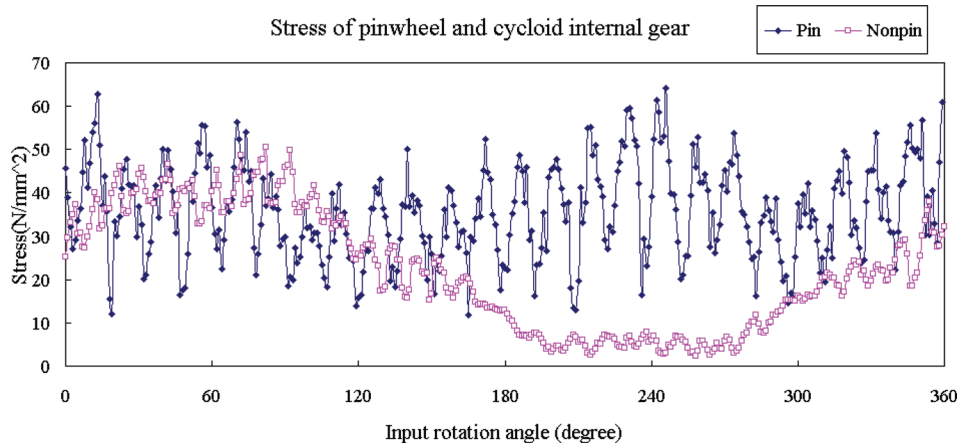


Fig. 14 Stress of pinwheel and cycloid internal gear

used for torsion testing the speed reducers is shown in Fig. 18. For this experiment, a motor with 0.18 kW power was connected to the reducer's input end, with an actual rotational speed of approximately 1640 rpm. Using the reduction ratio of 35:1, the theoretical output torque is 36.68 N m (T_{theo}). The test produced the following results: The average value of the output

torque (T_{ave}) of the pin design was 34.335 N m with an output rate of 93.6% ($(T_{\text{ave}}/T_{\text{theo}} \times 100\%)$) while that of the nonpin design was 35.08 N m with a single-stage output rate of 95.6% (Fig. 19). As is apparent, the nonpin design achieves larger output torque, which is consistent with the prediction of the simulation.

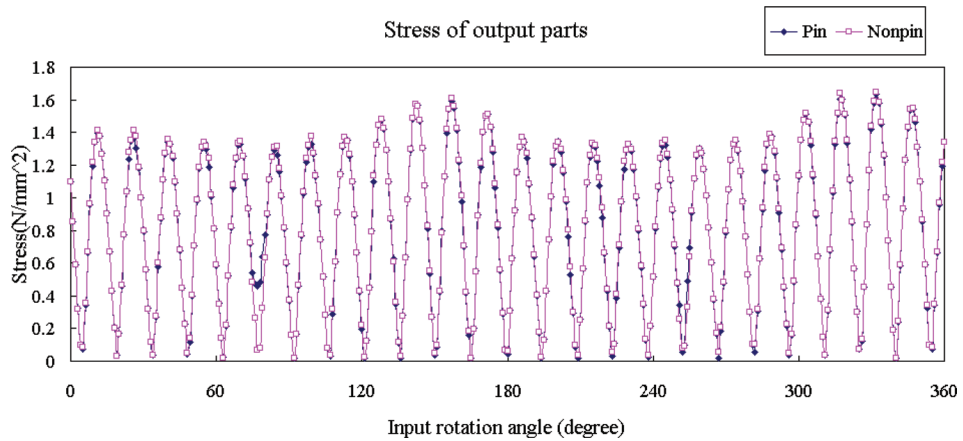


Fig. 15 Stress of output parts

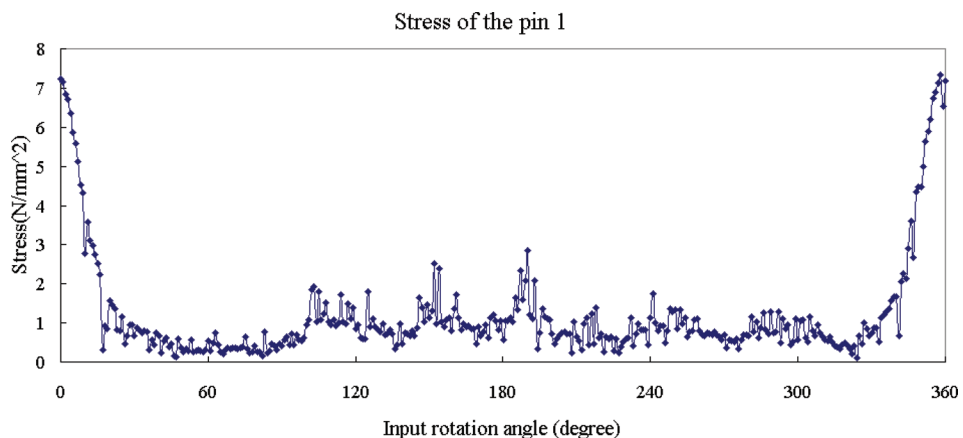


Fig. 16 Stress of the pin 1

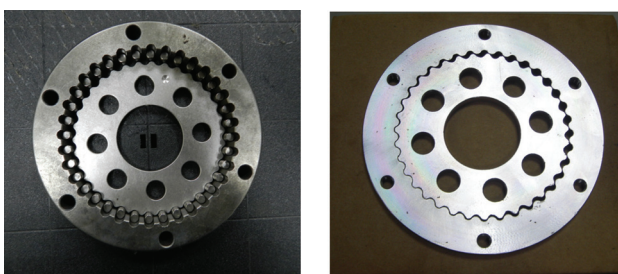


Fig. 17 Processed products of main parts: (a) pin design and (b) nonpin design

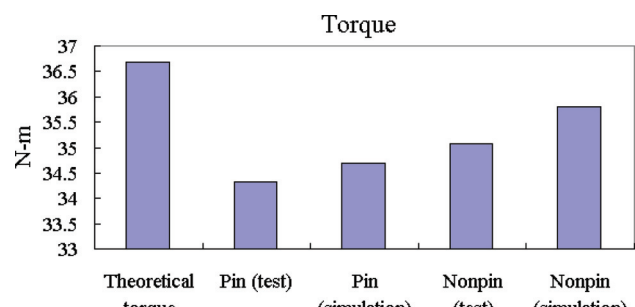


Fig. 19 Comparison of torsion

4 Conclusions

In this study, a system dynamics analysis model of a cycloidal speed reducer was developed and then, using a tooth number difference of 1 and reduction ratio of 35:1 as an example, the effects of the pin and nonpin designs on the speed reducer's dynamics were compared. In the pin design, when the cycloidal gear rotates at high speed, the pins sway slightly because of collision. This design may therefore lead to more collision during operation and reduce transmission performance. The dynamics analysis also demonstrated that the pin design produces a more substantial amount of vibration and significantly greater stress fluctuation than the nonpin design. An additional output torque simulation further predicted that the nonpin design would be superior to the pin design and could improve on the pin design's defects. The accuracy of these simulation predictions was verified using a



Fig. 18 Experimental equipment

practical manufacturing test. The results of both the simulations and the practical experiment suggest that the system dynamics model developed here can accurately assess speed reducer performance and facilitate the development of high-performance mechanisms.

Acknowledgment

The author is grateful to the Six Stars Company in Taiwan for their grant and their help with products, manufacturing, and torsion test. Part of this work has performed under Contract No. 100 AF50.

References

- [1] Blanche, J. G., and Yang, D. C. H., 1989, "Cycloid Drives With Machining Tolerances," *ASME J. Mech. Des.*, **111**(3), pp. 337–344.
- [2] Yang, D. C. H., and Blanche, J. G., 1990, "Design and Application Guidelines for Cycloid Drives With Machining Tolerances," *Mech. Mach. Theory*, **25**(5), pp. 487–501.
- [3] Shung, J. B., and Pennock, G. R., 1994, "Geometry for Trochoidal-Type Machines With Conjugate Envelopes," *Mech. Mach. Theory*, **29**(1), pp. 25–42.
- [4] Litvin, F. L., and Feng, P. H., 1996, "Computerized Design and Generation of Cycloidal Gearings," *Mech. Mach. Theory*, **31**(7), pp. 891–911.
- [5] Litvin, F. L., Demenego, A., and Vecchiato, D., 2001, "Formation by Branches of Envelope to Parametric Families of Surfaces and Curves," *Comput. Methods Appl. Mech. Eng.*, **190**, pp. 4587–4608.
- [6] Yan, H. S., and Lai, T. S., 2002, "Geometry Design of an Elementary Planetary Gear Train With Cylindrical Tooth Profiles," *Mech. Mach. Theory*, **37**(8), pp. 757–767.
- [7] Li, X., He, W., Li, L., and Schmidt, L. C., 2004, "A New Cycloid Drive With High-Load Capacity and High Efficiency," *ASME J. Mech. Des.*, **126**(4), pp. 683–686.
- [8] Shin, J. H., and Kwon, S. M., 2006, "On the Lobe Profile Design in a Cycloid Reducer Using Instant Velocity Center," *Mech. Mach. Theory*, **41**(5), pp. 596–616.
- [9] Mimmi, G. C., and Pennacchi, P. E., 2000, "Non-Undercutting Conditions in Internal Gears," *Mech. Mach. Theory*, **35**(4), pp. 477–490.
- [10] Fong, Z. H., and Tsay, C. W., 2000, "Study on the Undercutting of Internal Cycloidal Gear With Small Tooth Difference," *J. Chin. Soc. Mech. Eng.*, **21**(4), pp. 359–367.
- [11] Hwang, Y. W., and Hsieh, C. F., 2007, "Geometric Design Using Hypotrochoid and Non-undercutting Conditions for an Internal Cycloidal Gear," *ASME J. Mech. Des.*, **129**(4), pp. 413–420.
- [12] Hwang, Y. W., and Hsieh, C. F., 2007, "Determination of Surface Singularities of a Cycloidal Gear Drive With Inner Meshing," *Math. Comput. Model.*, **45**(4), pp. 340–354.
- [13] Chen, G., Zhong, H., Liu, J., Li, C., and Fang, T., 2012, "Generation and Investigation of New Cycloid Drive With Double Contact," *Mech. Mach. Theory*, **49**(3), pp. 270–283.
- [14] Malhotra, S. K., and Parameswaran, M. A., 1983, "Analysis of a Cycloid Speed Reducer," *Mech. Mach. Theory*, **18**(6), pp. 491–499.
- [15] Yunhong, M., Changlin, W., and Liping, L., 2007, "Mathematical Modeling of the Transmission Performance of 2K-H Pin Cycloid Planetary Mechanism," *Mech. Mach. Theory*, **42**(7), pp. 776–790.
- [16] Gorla, C., Davoli, P., Rosa, F., Longoni, C., Chiozzi, F., and Samarani, A., 2008, "Theoretical and Experimental Analysis of a Cycloidal Speed Reducer," *ASME J. Mech. Des.*, **130**(11), p. 112604.
- [17] Kahraman, A., Ligata, H., and Singh, A., 2010, "Influence of Ring Gear Rim Thickness on Planetary Gear Set Behavior," *ASME J. Mech. Des.*, **132**(2), p. 021002.
- [18] Blagojevic, M., Marjanovic, N., Djordjevic, Z., Stojanovic, B., and Disic, A., 2011, "A New Design of a Two-Stage Cycloidal Speed Reducer," *ASME J. Mech. Des.*, **133**(8), p. 085001.
- [19] Sensinger, J. W., 2010, "Unified Approach to Cycloid Drive Profile, Stress, and Efficiency Optimization," *ASME J. Mech. Des.*, **132**(2), p. 024503.
- [20] Sensinger, J. W., 2013, "Efficiency of High-Sensitivity Gear Trains, Such as Cycloid Drives," *ASME J. Mech. Des.*, **135**(7), p. 071006.
- [21] Sensinger, J. W., and Lipsey, J. H., 2012, "Cycloid vs. Harmonic Drives for Use in High Ratio, Single Stage Robotic Transmissions," *IEEE Conference on Robotics and Automation, St. Paul, MN*, pp. 4130–4135.
- [22] Ivanović, L., Devedžić, G., Ćuković, S., and Mirić, N., 2012, "Modeling of the Meshing of Trochoidal Profiles With Clearances," *ASME J. Mech. Des.*, **134**(4), p. 041003.
- [23] Litvin, F. L., 1994, *Gear Geometry and Applied Theory*, Prentice Hall, New York.
- [24] He, B., Wang, G. P., and Rui, X. T., 2008, *Transfer Matrix Method of Multi-body System and Its Applications*, Science Press Ltd., Beijing, China.